Zero-baseline Analysis of GPS/BeiDou/Galileo Between-Receiver Differential Code Biases (BR-DCBs): Time-wise Retrieval and Preliminary Characterization

B. Zhang[1], P.J.G. Teunissen[1,2]
[1]*GNSS Research Centre, Curtin University, Australia*
[2]*Geoscience and Remote Sensing, delft University of Technology, The Netherlands*

BIOGRAPHY

Baocheng Zhang is a research fellow in the GNSS Research Centre at Curtin University. His research is focused on multi-GNSS integer ambiguity resolution enabled Precise Point Positioning (PPP-RTK), with an emphasis on code and carrier-phase bias estimation and characterization, ionospheric delay retrieval and prototype PPP-RTK network software development.

Peter J.G. Teunissen is Science Director of the CRC-SI, Professor of Geodesy and Navigation and Head of Curtin's GNSS Research Centre. His current research focus is on modeling next-generation GNSS for improved parameter estimation and validation.

ABSTRACT

When sensing the Earth's ionosphere using multiple Global Navigation Satellite Systems (GNSSs) special care needs to be taken of the receiver Differential Code Bias (DCB) contributions to the error budget. For this reason timely and accurate retrieval of multi-GNSS receiver DCBs with the goal of gaining insight into their characteristics would be of relevance. In this contribution we propose a method able to time-wisely retrieve the Between-Receiver DCBs (BR-DCBs) from code measurements collected by a zero-baseline setup, thereby eliminating most common error sources. We base our investigations on dual-frequency GPS (L1+L2), BeiDou (B1+B2) and Galileo (E1+E5a) measurements collected in 2013 with a 30 second sampling rate by four geodetic grade receivers (two Trimble NETR9s, one Septentrio POLARX4 and one Javad TRE-G3TH) connected to one common antenna. For each receiver-pair, we process the GPS/GEO/IGSO/MEO/Galileo measurements separately and then obtain the time-wise estimates of five groups of BR-DCBs. With the use of statistical hypothesis testing schemes, we confirm that: (1). the time-wise estimates of BR-DCBs for all tested receiver-pairs exhibit good intra-day stability; and (2). the daily weighted average (DWA) estimates of GEO/IGSO/MEO BR-DCBs are inconsistent for receiver-pairs of mixed type, due to the presence of BeiDou code Inter-Satellite-Type-Biases (ISTBs). We also identify likely factors accounting for the variability in the DWA estimates of BR-DCBs over a 1-year interval as: (1). receiver firmware upgrades; and (2). daily maximum temperature variations at receiver sites.

INTRODUCTION

The space-borne and ground-based Global Navigation Satellite System (GNSS) measurements with extensive spatial coverage and high temporal resolution are particularly ideal data sources for studying the ionosphere [1]. Over the past few decades, the ionospheric information retrieved from the GPS measurements broadcast at two frequencies has enabled us to understand the intrinsic mechanisms of the space weather effects [2, 3], to explore the potential causes of the seismic hazards [4, 5], and to improve the empirical precision of space geodetic applications [6]. In addition to the GPS that is undergoing uninterrupted modernization, the Chinese BeiDou and the European Galileo are currently under development for global operation as well [7]. So far, the BeiDou constellation consisting of 14 satellites in orbit (five GEO + five IGSO + four MEO) has become operational in the Asian-Pacific region [8]. The Galileo is still in the deployment phase and currently has four In-Orbit-Validation (IOV) satellites operating. The remaining Galileo satellites will soon be launched, in order to complete the constellation for the Full Operational Capability (FOC) phase [9]. With these general facts in mind, one would expect that the available multi-GNSS data sets would allow us to acquire much deeper insight into the actual state of the ionosphere than before [10, 11].

Precise estimation of vertical Total Electron Content (vTEC) parameters from dual- or multi-frequency GNSS measurements is a crucial prerequisite for GNSS-based ionosphere studies [12]. For this purpose one has to tackle the satellite and receiver Differential Code Bias (DCB) contributions to the error budget [13]. The near constant space environment onboard the GNSS constellation gives rise to fairly promising long-term stability of the satellite DCBs [14, 15]. As a consequence, we would be able to determine the satellite DCBs with relatively high accuracy (as good as 0.1 ns) and thus get rid of their impact on the estimated vTEC easily [16, 17]. In contrast,

however, one may experience significant single-receiver (absolute) or/and between-receiver (relative) DCB variations during a time period of one day or even a few hours, possibly caused by the changing temperature conditions at the receiver antenna, along the cable, or in the internal receiver hardware [18, 19]. Such temporal variability of receiver DCBs, if not circumvented properly, will partially account for both the levelling errors underlying the line-of-sight ionospheric observables [20], as well as the vTEC modelling errors [21-23].

With the ultimate goal of improving the reliability of vTEC estimation, so far a variety of approaches have been proposed to determine the characteristics (typically the stability) of the receiver DCBs retrieved either from the vTEC estimation process as a by-product [24, 25], or from differencing the ionospheric observables determined for two co-located receivers [20, 26]. However, for the following two reasons these approaches may still be inadequate. First, when using such methods the retrieved receiver DCBs may still be affected by un-modelled biases. Second, the so-obtained time series of receiver DCBs are usually of low time resolution (a few hours to one day) and may thus fail to identify any possible receiver DCB variations over shorter time intervals (e.g. less than 1 hour).

In this contribution, we first develop an approach for retrieving Between-Receiver DCBs (BR-DCBs) based on a zero-baseline set up. Without relying on the vTEC estimation process or the formation of ionospheric observables, our approach is able to achieve time-wise BR-DCB retrieval by employing only a single epoch of between-receiver, between-frequency double-differenced (DD) GNSS code measurements. Owing to the fact that for zero-baseline most common error sources are actually cancelled out in our DD code measurements [27], the residual error sources affecting our BR-DCB retrieval can thereby be minimized. With the use of dual-frequency GPS/BeiDou/Galileo measurements collected in 2013 with a sampling rate of 30 seconds by four multi-GNSS receivers connected to one common antenna, we then investigate: (1). the intra-day stability in the time-wise estimates of BR-DCBs; (2). the consistency between the daily weighted average (DWA) estimates of GEO/IGSO/MEO BR-DCBs for a common receiver-pair; (3). the factors accounting for the variability in the DWA estimates of BR-DCBs.

METHOD DESCRIPTION

In this section, we outline the procedure of our time-wise BR-DCB retrieval approach. Next to that, we briefly illustrate two statistical hypothesis testing schemes that are adopted to validate the intra-day stability in time-wise estimates of BR-DCBs and the consistency between DWA estimates of GEO/IGSO/MEO BR-DCBs.

Time-wise BR-DCB retrieval

Let us assume that, at certain epoch i, two receivers forming a zero-baseline are able to simultaneously track several GNSS satellites at two frequencies. With respect to one satellite s, its between-receiver single-differenced (SD) code observation equations take the form

$$E\left\{p_j^{s,G}(i)\right\} = dt^G(i) + b_j^G(i) \tag{1}$$

where $E\{\cdot\}$ denotes the expectation operator, $j = 1,2$ denotes the frequency index, $p_j^{s,G}(i)$ denotes the dual-frequency SD code measurements for satellite s that belongs to GNSS constellation G transmitting code division multiple access (CDMA) signals. Unknown parameters are: $dt^G(i)$ the SD receiver clock, $b_j^G(i)$ the frequency-dependent SD receiver code biases.

The system of observation equations represented by (1) is not solvable, since all the unknown parameters are not individually estimable. For this reason we further difference the SD code observation equations between two frequencies and eventually get

$$E\left\{p_{12}^{s,G}(i)\right\} = b_{12}^G(i) \tag{2}$$

where $p_{12}^{s,G}(i) = p_1^{s,G}(i) - p_2^{s,G}(i)$ is the DD code measurement and $b_{12}^G(i) = b_1^G(i) - b_2^G(i)$ is the BR-DCB parameter of our interest.

The formal precision of $p_{12}^{s,G}(i)$ can be given as

$$D\left\{p_{12}^{s,G}(i)\right\} = \left[\frac{2\sigma^{s,G}}{\sin\left\{\theta^{s,G}(i)\right\}}\right]^2 \tag{3}$$

where $D\{\cdot\}$ is the dispersion operator, $\sigma^{s,G}$ denotes the zenith-referenced undifferenced code standard deviation, $\theta^{s,G}(i)$ denotes the elevation angle of satellite s at epoch i.

At every epoch, after setting up the functional (stochastic) models similar to (2) ((3)) for all the satellites belonging to one common constellation, we can readily retrieve the BR-DCBs, along with their formal precision, using the least-square estimator. The epoch-wise least-squares solution is therefore a weighted average over all satellites, in which the reciprocal value of (3) is used as weighting.

We remark that, when applying the BR-DCB retrieval approach described above to BeiDou constellation, one should be aware of the possible presence of the code Inter-Satellite-Type-Biases (ISTBs) for receiver-pairs of mixed type [28]. According to [29], the existence of code ISTBs could not be clearly explained by receiver design parameters. One possible cause might be a bias induced by the multipath for the GEO satellites which is constant and receiver dependent. By definition, the BeiDou code ISTBs associated with two satellite types, denoted as $B_j^{gm}(i)$, can be interpreted as

$$B_j^{gm}(i) = b_j^g(i) - b_j^m(i) \tag{4}$$

where $b_j^g(i)$ ($b_j^m(i)$) denotes the SD receiver code biases involved in the SD code observation equations formulated for satellite type g (m).

Further differencing $B_j^{gm}(i)$ at two frequencies will yield the following identity

$$B_1^{gm}(i) - B_2^{gm}(i) = \left[b_1^g(i) - b_2^g(i)\right] - \left[b_1^m(i) - b_2^m(i)\right] \quad (5)$$

where $b_1^g(i) - b_2^g(i)$ and $b_1^m(i) - b_2^m(i)$ are in fact the BeiDou BR-DCBs retrieved by DD code measurements belonging to satellite types g and m, respectively. From (5) it follows that, would dual-frequency BeiDou code ISTBs be present and different, one has to retrieve satellite type dependent BeiDou BR-DCBs.

Finally, it is worth mentioning that our time-wise BR-DCB retrieval approach is unlikely to benefit from further involvement of the carrier-phase measurements. Usually, this fact holds true in the case where the real-valued ambiguity parameters are estimated (ambiguity-float scenario). Moreover, even if the (between-receiver, between-satellite) DD ambiguity parameters have been successfully resolved into integers (ambiguity-fixed scenario), the contribution of incorporating carrier-phase measurements to the BR-DCB retrieval is still virtually negligible [30].

Statistical hypothesis testing

With a total of t time-wise estimates of BR-DCBs over one day available, the DWA estimate of them, denoted as $\bar{b}_{12}^G$, can be calculated as follows

$$\bar{b}_{12}^G = \frac{\sum_{i=1}^{t} b_{12}^G(i) \big/ \sigma_{b_{12}^G}^2(i)}{\sum_{i=1}^{t} 1 \big/ \sigma_{b_{12}^G}^2(i)} \quad (6)$$

where $b_{12}^G(i)$ is weighted according to its formal precision $\sigma_{b_{12}^G}^2(i)$.

In addition, with the use of the error propagation law, we can also obtain the formal precision of $\bar{b}_{12}^G$ which is denoted as $\sigma_{\bar{b}_{12}^G}^2$ and reads

$$\sigma_{\bar{b}_{12}^G}^2 = \frac{1}{\sum_{i=1}^{t} 1 \big/ \sigma_{b_{12}^G}^2(i)} \quad (7)$$

It is remarked that computation of $b_{12}^G(i)$ and $\sigma_{\bar{b}_{12}^G}^2$ as given above will form the basis for our illustration of two statistical hypothesis testing schemes in the following.

Test statistic T_s used to diagnose the intra-day stability of $b_{12}^G(i)$ can be constructed as

$$T_s = \sum_{i=1}^{t} \frac{\left(b_{12}^G(i) - \bar{b}_{12}^G\right)^2}{\sigma_{b_{12}^G}^2(i)} \quad (8)$$

where T_s is Chi-square distributed with $t-1$ degrees of freedom, assuming that $b_{12}^G(i)$ is normally distributed. The critical value of T_s can be written as $\chi_{\alpha_s}^2(t-1,0)$ in which the level of significance is set to α_s. One would conclude that $b_{12}^G(i)$ does not exhibit any significant changes over time if $T_s < \chi_{\alpha_s}^2(t-1,0)$ occurs.

In parallel, in order to ascertain the possible dependency of BeiDou BR-DCBs upon the satellite type, we construct the following test statistic T_c which reads

$$T_c = \frac{\bar{b}_{12}^g - \bar{b}_{12}^m}{\sqrt{\sigma_{\bar{b}_{12}^g}^2 + \sigma_{\bar{b}_{12}^m}^2}} \quad (9)$$

where $\bar{b}_{12}^g$ ($\bar{b}_{12}^m$) denote the DWA estimate of $\left[b_1^g(i) - b_2^g(i)\right]$ ($\left[b_1^m(i) - b_2^m(i)\right]$, *cf.* equation 5), while its formal precision is given as $\sigma_{\bar{b}_{12}^g}^2$ ($\sigma_{\bar{b}_{12}^m}^2$). T_c has a standard normal distribution. One would decide for a significant difference between $\bar{b}_{12}^g$ and $\bar{b}_{12}^m$ if $|T_c| > N_{0.5\alpha_c}(0,1)$ holds for a given significance level α_c.

EXPERIMENTAL ANALYSIS

Data preparation and processing

Fig. 1 Curtin GNSS geodetic grade antenna (*CUT00*) and four multi-GNSS receivers of three types (*given in brackets*) used in this study. *Top* antenna setup with SCIS radome. *Bottom* receiver–antenna connectivity

The experimental data sets are measured by four multi-GNSS receivers from the GPS (L1+L2), the BeiDou (B1+B2) and the Galileo (E1+E5a) constellations in 2013 with a sampling rate of 30 seconds and a cut-off elevation angle of 15 degrees. As shown in Fig. 1, all the receivers are placed at the main campus of Curtin University in Bentley (Perth) and commonly connected to a Trimble TRM 59800.00 geodetic grade antenna with SCIS radome. Table 1 presents an overview of the basic characteristics of the four receivers, while Table 2 summarizes the signals of the dual-frequency, multi-GNSS code measurements used.

Table 1 Four experimental multi-GNSS receiver characteristics

Receiver name	Receiver type	Antenna type	Remark
CUT0 (*pivot*)	Trimble NETR9	TRM59800.00 SCIS	firmware version was upgraded from 4.70 to 4.80 at day 175, 2013
CUT1	Septentrio POLARX4		
CUT2	Trimble NETR9		the same firmware version upgrade process as CUT0
CUT3	Javad TRE-G3TH		removed during days 242-246 and days 254-261, 2013

We define three independent receiver-pairs, all referring to the CUT0 as pivot receiver. For each of them we time-wisely retrieve five groups of BR-DCBs using the GPS/GEO/IGSO/MEO/Galileo code measurements, respectively. We emphasize here again that, to investigate the possible dependency of BeiDou BR-DCBs upon the satellite type, the code measurements from BeiDou GEO/IGSO/MEO satellites are processed separately, as if they were from three different constellations.

Table 2 Overview of dual-frequency, multi-GNSS code measurements used in this study

Syst.	Band	Frequency (MHz)	Component
GPS	L1	1575.42	C
	L2	1227.60	W
BeiDou	B1	1561.098	I
	B2	1207.14	I
Galileo	E1	1575.42	X: CUT0, CUT3 C: CUT1, CUT2
	E5a	1176.45	X: CUT0, CUT3 Q: CUT1, CUT2

For the zenith-referenced undifferenced code standard deviations we use the value of 30 cm, which is a reasonable approximation to the empirical values estimated using multi-GNSS data from the same receivers [31, 32]. We derive the satellite positions that are basic inputs to elevation angle computation from the broadcast ephemerides. We remark that, receiving broadcast ephemerides from BeiDou (Galileo) constellation by at least one of our experimental receivers becomes possible only after day 49 (17) of 2013. When we compute the critical value for test statistic T_s (T_c), the level of significance α_s (α_c) is chosen equal to 5%.

We shall for the sake of brevity restrict our presentation to a selected set of representative BR-DCB results. All conclusions drawn about the characteristics of the presented BR-DCBs hold true for the rest of our BR-DCB results as well.

Analysis of intra-day stability in time-wise estimates of BR-DCBs

We first test the time-wise estimates of CUT0-CUT1 (*Trimble-Septentrio*) Galileo BR-DCBs and depict a series of computed test statistics T_s (*blue circles*) along with their critical values $\chi^2_{\alpha_s}(t-1,0)$ (*red dots*) in Fig. 2. A few gaps present in the time series of T_s ($\chi^2_{\alpha_s}(t-1,0)$) correspond to the time periods without navigation ephemerides (e.g. days 1-17) or lack of visible IOV satellites above cut-off elevation angle. Due to the fact that we assign a fixed value (5%) to the level of significance α_s, the values computed for $\chi^2_{\alpha_s}(t-1,0)$ are thereby solely driven by the degree of freedom $(t-1)$ and may vary dramatically from day to day. For those days (e.g. 253-289) when only one IOV satellite is intermittently visible the values taken by $\chi^2_{\alpha_s}(t-1,0)$ can drop down to 500 or even smaller. Quite clearly, it follows here that $T_s < \chi^2_{\alpha_s}(t-1,0)$ always holds true for all the testing days and thus can be taken as indication of intra-day stability in the time-wise estimates of BR-DCBs considered here.

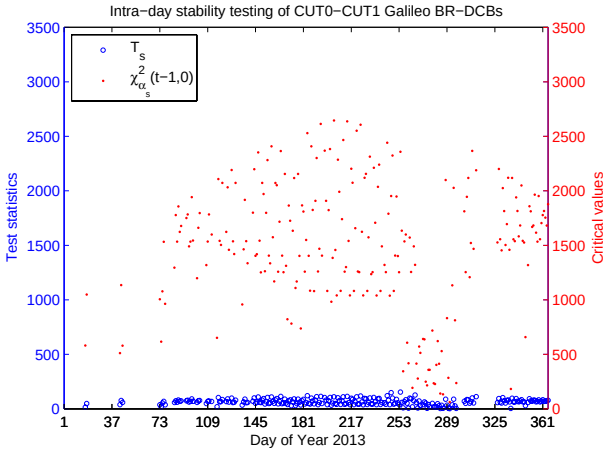

Fig. 2 Test statistics T_s (*blue circles*) used to diagnose the intra-day stability in the time-wise estimates of CUT0-CUT1 Galileo BR-DCBs. Critical values $\chi^2_{\alpha_s}(t-1,0)$ (*red dots*) computed using level of significance $\alpha_s = 5\%$, together with the degree of freedom $(t-1)$

Similarly, Figure 3 presents the statistical hypothesis testing results for diagnosing the intra-day stability in the time-wise estimates of CUT0-CUT2 (*Trimble-Trimble*) GPS BR-DCBs. Contrary to Fig. 2 in which the $\chi^2_{\alpha_s}(t-1,0)$ varies remarkably, it follows here that the values of $\chi^2_{\alpha_s}(t-1,0)$ stay almost constant over the entire one year period, mainly due to the nearly invariant $(t-1)$ ranging from 2850 to 2879. Again, we see from Fig. 3 that, the computed values of T_s (<500) are always

significantly smaller than that of $\chi^2_{\alpha_s}(t-1,0)$ (>3000). This confirms that the time-wise estimates of BR-DCBs tested here are sufficiently stable over every single day of 2013.

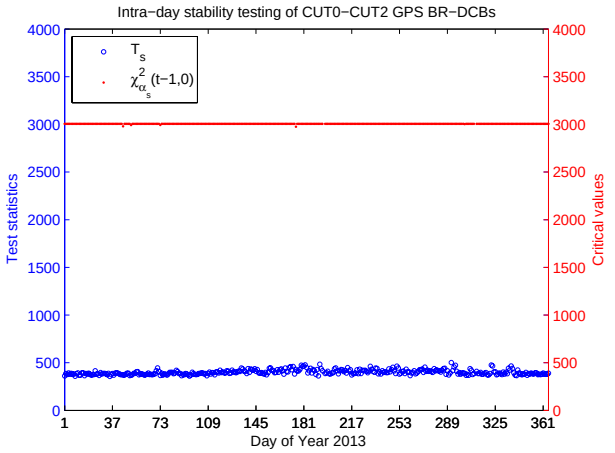

Fig. 3 Test statistics T_s (*blue circles*) used to diagnose the intra-day stability in the time-wise estimates of CUT0-CUT2 GPS BR-DCBs. Critical values $\chi^2_{\alpha_s}(t-1,0)$ (*red dots*) computed using level of significance $\alpha_s = 5\%$, together with the degree of freedom $(t-1)$

We remark that our test statistics only have a chi-square distribution if the BR-DCB estimators are normally distributed. We verify this by displaying first of all the Galileo BR-DCB estimates retrieved at day 211 as a histogram in Fig. 4 (*subplot a*), which has 2354 samples and 40 bins of width 0.15 ns. Also, we depict therein the empirical probability density function (PDF) of $N(0.26, 0.57)$ as a red curve, which corresponds to the empirical mean (0.26 ns) and the empirical standard deviation (0.57 ns) of those samples. Generally, we can recognize from subplot (a) that the histogram fits reasonably well with the empirical normal PDF, thereby implying the BR-DCB estimates retrieved at this day indeed obey a normal distribution. However, we have to point out that, the histogram seems to be slightly asymmetric as these estimates are heterogeneous in their formal precision. Furthermore, we use the Quantile-Quantile (QQ) plot (*subplot b*) as another tool to graphically demonstrate the close-to-normality of samples depicted in subplot (a). In such a QQ plot, the ordered samples are plotted against the quantiles of the empirical normal distribution $N(0.26, 0.57)$. Similar to what we have learnt from subplot (a), the linearity of the blue crosses shown in subplot (b) also suggests that the samples are close-to-normally distributed.

Additionally, we address in Fig. 5 the histogram of time-wise estimates of GPS BR-DCBs retrieved at day 71 (*subplot a*) as well as the corresponding QQ plot (*subplot b*). Considering first the subplot (a), the histogram has a total of 2880 samples and 40 bins of width 0.15 ns. The empirical normal PDF, determined by the empirical mean (0.64 ns) and the empirical standard deviation (0.42 ns) of these samples, is depicted as a red curve. In contrast to what we see from subplot (a) of Fig. 4, the conformity between the histogram and the empirical normal PDF becomes more evident. Moreover, since these BR-DCB estimates are more homogeneous in their formal precision the histogram is less asymmetric. With respect to the QQ plot depicted in subplot (b), the linearity of green crosses confirms the normal distribution of the samples as well.

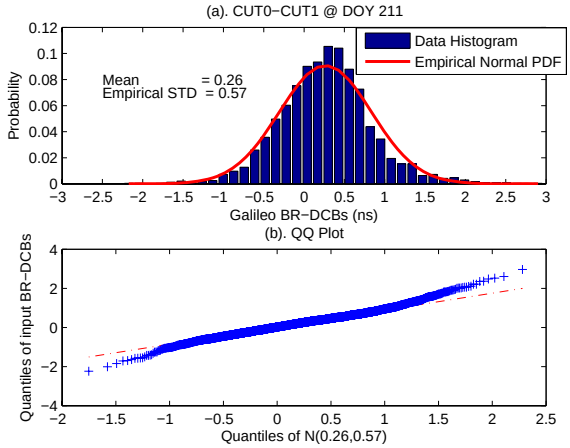

Fig. 4 *Panel (a)*: The histogram of time-wise estimates of Galileo BR-DCBs referring to day 211 and receiver-pair of CUT0-CUT1: 2354 samples and 40 bins of width 0.15 ns, and the empirical theoretical normal distribution (*red curve*) based on the mean (*0.26 ns*) and empirical standard deviation (*0.57 ns*) of the samples. *Panel (b)*: QQ plot of samples versus normal distribution $N(0.26, 0.57)$

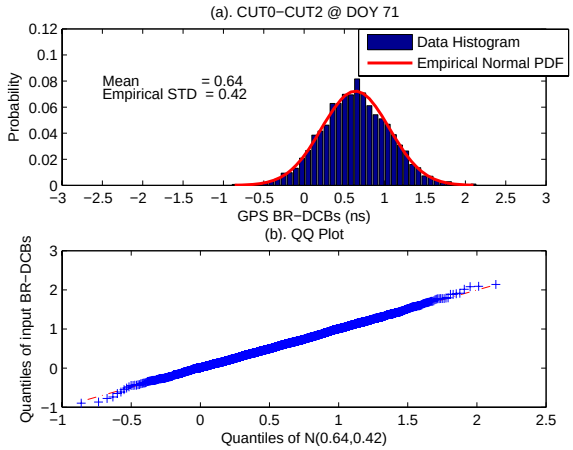

Fig. 5 *Panel (a)*: The histogram of time-wise estimates of GPS BR-DCBs referring to day 71 and receiver-pair of CUT0-CUT2: 2880 samples and 40 bins of width 0.15 ns, and the empirical theoretical normal distribution (*red curve*) based on the mean (*0.64 ns*) and empirical standard deviation (*0.42 ns*) of the samples. *Panel (b)*: QQ plot of samples versus normal distribution $N(0.64, 0.42)$

Possible dependency of BeiDou BR-DCB estimates upon satellite type

As inferred from (5), the BeiDou BR-DCBs would become dependent on satellite type, provided that the

dual-frequency code ISTBs are present and in the meantime differ from each other. We will verify this finding here by means of investigating the consistency between the DWA estimates of GEO/IGSO/MEO BR-DCBs retrieved for two receiver-pairs, involving not only the CUT0-CUT3 of mixed type (*Trimble-Javad, ISTB-affected*), but the CUT0-CUT2 of common type (*Trimble-Trimble, ISTB-free*) as well. We further remark that, with respect to CUT0-CUT3, the empirical values of dual-frequency BeiDou code ISTBs associated with any two satellite types are already made available by [28] (*cf. Table 5 therein*), thus offering us an opportunity to quantitatively validate (5).

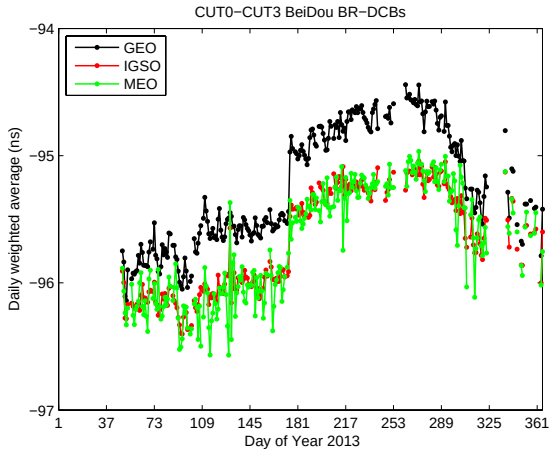

Fig. 6 The daily weighted average estimates of CUT0-CUT3 (*Trimble-Javad*) BeiDou BR-DCBs in 2013: GEO results (*black dotted line*), IGSO results (*red dotted line*) and MEO results (*green dotted line*)

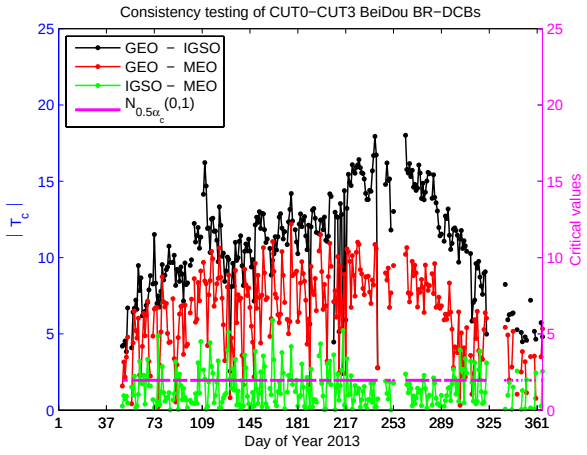

Fig. 7 Three test statistics $|T_c|$ (*black/red/green dotted lines*) used to diagnose the consistency between CUT0-CUT3 GEO/IGSO/MEO BR-DCBs (*cf. Fig. 6*). Critical value $N_{0.5\alpha_c}(0,1)$ (*magenta line*) computed using level of significance $\alpha_c = 5\%$

We show in Fig. 6 the DWA estimates of GEO/IGSO/MEO BR-DCBs retrieved for CUT0-CUT3. It follows that, the time series of IGSO BR-DCBs (*dotted red line*) is generally in good agreement with that of MEO BR-DCBs (*dotted green line*). The mean value of their difference amounts to -0.02 ns (-0.6 cm), which is very close to the difference between the empirical values of dual-frequency IGSO-MEO code ISTBs (-1 cm) as reported in [28]. However, in contrast to the other two time series, the time series of GEO BR-DCBs (*dotted black line*) is found to have a constant offset of roughly 0.45 ns (13.5 cm), which deviates slightly from the difference between the empirical values of dual-frequency GEO-MEO (GEO-IGSO) code ISTBs (9 cm) as reported in [28]. Therefore, one should be aware that the BeiDou code ISTBs may lead to inconsistent GEO/IGSO/MEO BR-DCBs in their DWA estimates.

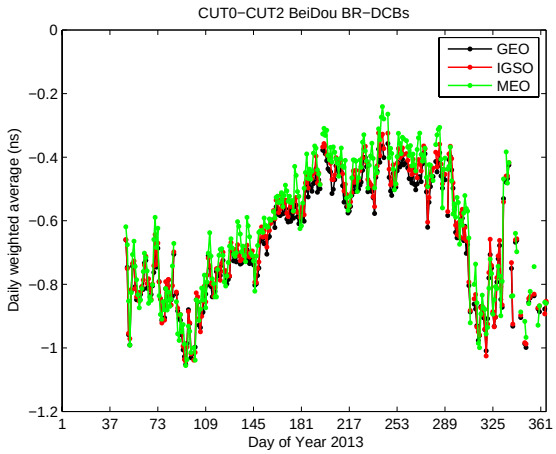

Fig. 8 The daily weighted average estimates of CUT0-CUT2 (*Trimble-Trimble*) BeiDou BR-DCBs in 2013: GEO results (*black dotted line*), IGSO results (*red dotted line*) and MEO results (*green dotted line*)

With the use of (9), we test whether the discrepancy between any two of the time series given in Fig. 6 is statistically significant or not. For each day we compute three test statistics T_c and present their absolute values $|T_c|$ in Fig. 7. Also, a series of critical values $N_{0.5\alpha_c}(0,1) = 1.96$ remaining constant over all 260 days are depicted as a magenta line. From these findings we conclude that for receiver-pair CUT0-CUT3 the DWA estimates of GEO BR-DCBs are essentially different from that of IGSO/MEO BR-DCBs.

Quite similar to Fig. 6, we show in Fig. 8 the DWA estimates of GEO/IGSO/MEO BR-DCBs retrieved for the other receiver-pair CUT0-CUT2 that is found to be free from BeiDou code ISTBs. In this case, we see that three time series agree fairly well with one another, which suggests good consistency between GEO/IGSO/MEO BR-DCB estimates for CUT0-CUT2. This finding is further verified by the statistical hypothesis testing results presented in Fig. 9, in which the computed values of all T_c are well below 1.96 with quite rare exceptions.

The discussions above would enable us to draw a preliminary conclusion. When retrieving the BeiDou BR-DCBs for receiver-pairs of mixed type, one should take special care of the effect due to the code ISTBs that may be present. Provided that the dual-frequency code ISTBs deviates significantly from each other, it then requires one

to consider the dependency of BeiDou BR-DCBs upon satellite type. On the other hand, one can safely introduce satellite type independent BeiDou BR-DCBs for receiver-pairs of common type.

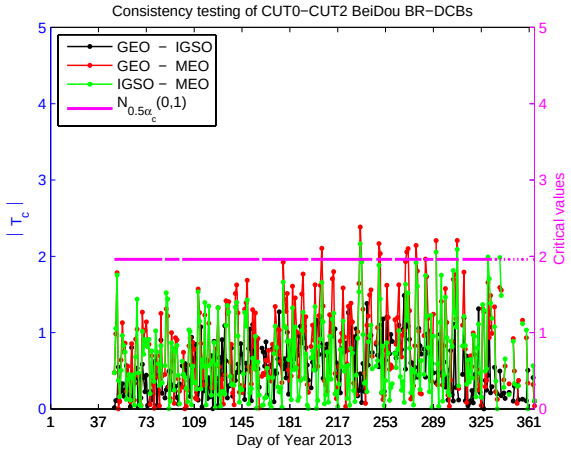

Fig. 9 Three test statistics $|T_c|$ (*black/red/green dotted lines*) used to diagnose the consistency between CUT0-CUT2 GEO/IGSO/MEO BR-DCBs (*cf. Fig. 8*). Critical value $N_{0.5\alpha_c}(0,1)$ (*magenta line*) computed using level of significance $\alpha_c = 5\%$

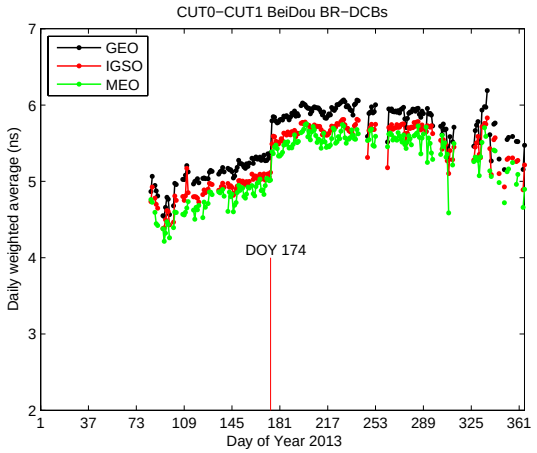

Fig. 10 The daily weighted average estimates of CUT0-CUT1 (*Trimble*-Septentrio) BeiDou BR-DCBs in 2013: GEO results (*black dotted line*), IGSO results (*red dotted line*) and MEO results (*green dotted line*). Only after day 84, CUT1 starts to receive signals from BeiDou IGSO and MEO satellites. The vertical red line indicates the day (*174*) when the firmware version of CUT0 was upgraded from 4.70 to 4.80

Analysis of inter-day variability in BR-DCB estimates

Although we did not mention it yet, one may recognize from Fig. 6 that an abrupt change occurs in the DWA estimates of CUT0-CUT3 BeiDou BR-DCBs before day 181, and from Fig. 8 that there is a trend in the time series of CUT0-CUT2 BeiDou BR-DCB estimates. We will attempt to seek for the possible reasons that account for the occurrence of such two phenomena. Before doing so, we present in Table 3 the statistics of the DWA estimates of 15 groups of BR-DCBs retrieved for all three receiver-pairs over 2013, in which the empirical standard deviation values would provide us an overall impression on the inter-day variability of each group of BR-DCB estimates. In general it follows from Table 3 that, with respect to a common constellation, the BR-DCB estimates retrieved for two receiver-pairs of mixed type (in particular CUT0-CUT3) always have larger empirical standard deviations than those for receiver-pair of common type (CUT0-CUT2), thus implying more evident inter-day variability. Moreover, in addition to CUT0-CUT3, GEO/IGSO/MEO BR-DCB estimates retrieved for CUT0-CUT1 also manifest obvious discrepancy in their mean values, which can also be attributed to BeiDou code ISTBs.

Similar to what one can see from Fig. 6, DWA estimates of CUT0-CUT1 BeiDou BR-DCBs depicted in Fig. 10 also exhibit an abrupt change. Both BD-DCB changes occur concurrently at day 175 and their actual sizes are roughly 0.5 ns and 0.4 ns, respectively. One very likely factor accounting for this may be identified as firmware version upgrade undergone by receiver CUT0 at day 174. The reason for this can be explained as follows. In general, the receiver code biases depend not only on the hardware, but also on the digital signal processing that may change with a firmware version upgrade [29]. Interestingly, we notice that all groups of CUT0-CUT2 BR-DCB estimates seem to have no explicit response to firmware version upgrade of CUT0. Considering the fact that the other receiver CUT2 was also upgraded at the same day and both receivers are of common type (*cf. Table 1*), the changes in their absolute DCBs caused by simultaneous firmware version upgrades would be identical and thus could not manifest themselves in the retrieved BR-DCB estimates.

According to the literature devoted to GNSS (albeit GPS-only) receiver DCB studies (e.g. [18, 19, 26, 33, 34]), the temperature is generally acknowledged as a predominant factor accounting for receiver DCB variations. With this in mind, we assume that the inter-day variability in DWA estimates of CUT0-CUT2 BeiDou BR-DCBs (*cf. Fig. 8*) is a direct consequence of varying temperature at the receiver sites. To verify our assumption, we depict in Fig. 11 the time series of CUT2-CUT0 GEO BR-DCB estimates (*dotted blue line*), together with that of daily maximum temperature (*dotted red line*) observed by a weather station deployed about 8 km away from our receiver sites. We determine the Pearson correlation coefficient (r) between the two time series to quantify their statistical dependence. For a statistical sample size greater than 100, as is the case here, the absolute value of r greater than 0.254 is rated significant. Here the computed Pearson r value is equal to 0.788 and the corresponding p-value for testing the null hypothesis of no correlation against the alternative that there is a nonzero correlation is fairly small (≈ 0). This shows that both time series are highly correlated and it thus suggests that the inter-day variability in BR-DCB estimates is indeed due to the temperature effect.

Table 3 Statistics of the DWA estimates of BR-DCBs over 2013: mean/empirical standard deviation (ns)

Receiver-pair	GPS	BeiDou			Galileo
		GEO	IGSO	MEO	
CUT0-CUT1 (Trimble-Septentrio)	-13.63/0.36	5.45/0.49	5.32/0.43	5.19/0.44	0.18/0.25
CUT0-CUT2 (Trimble-Trimble)	0.52/0.16	-0.65/0.18	-0.64/0.19	-0.62/0.20	0.35/0.11
CUT0-CUT3 (Trimble-Javad)	-13.13/0.82	-95.24/0.47	-95.67/0.40	-95.69/0.46	-12.88/1.80

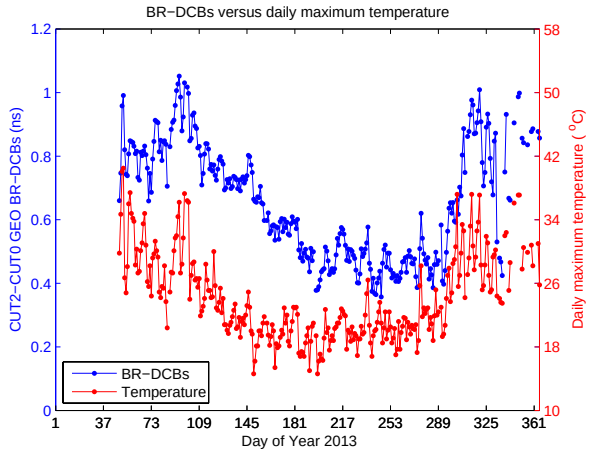

Fig. 11 The daily weighted average estimates of CUT2-CUT0 GEO BR-DCBs (*blue dotted line*) and the daily maximum temperature values (*red dotted line*) measured by a weather station deployed about 8 km away from the receiver site. The Pearson correlation coefficient between both time series is 0.788 with a corresponding p-value of almost zero

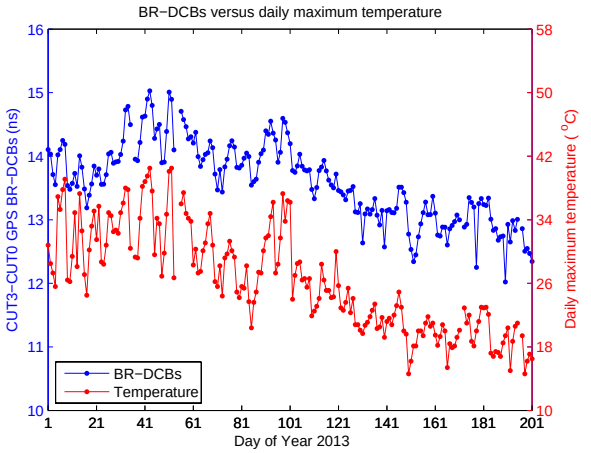

Fig. 12 The daily weighted average estimates of CUT3-CUT0 GPS BR-DCBs (*blue dotted line*) and the daily maximum temperature values (*red dotted line*) measured by a weather station deployed about 8 km away from the receiver site. The time period indicated by the horizontal axis corresponds to days 1-201 of 2013. The Pearson correlation coefficient between both time series is 0.90 with a corresponding p-value of almost zero

Recall that there exist three likely factors accounting for the receiver DCB dependence on temperature: the antenna, the cable and the receiver hardware [18]. For our zero-baseline setup, the cables can further be separated into one antenna-splitter cable commonly shared by all the receivers, as well as those splitter-receiver cables connecting the splitter to each receiver. One reason for having temperature effect zero-baseline BR-DCB estimates might be caused by reflections in the cables that depend on the antenna impedance and can slightly vary with temperature. Since the radio frequency paths along the cables to the two receivers are not exactly identical, these reflections would induce a different code bias on both receivers [29]. In this case, as both receivers are of common type (*Trimble NETR9*), one would surmise that a large proportion of the effect due to the temperature on their BR-DCB estimates should be largely cancelled [35]. This may explain why in this case the peak-to-peak variation between the highest and the lowest BR-DCB estimates is only about 0.6 ns.

Similarly, Figure 12 shows the CUT0-CUT3 GPS BR-DCB estimates for the first 201 days of 2013. Aside from that, the maximum temperature value at each day is also given. The Pearson r value determined for both time series is as great as 0.9 corresponding to a p-value of zero. This again clearly demonstrates the effect of temperature upon the inter-day variability in another group of BR-DCB estimates. Moreover, the peak-to-peak variation of BR-DCB estimates now reaches roughly 3 ns, possibly due to the fact that both receivers are of mixed type.

SUMMARY AND CONCLUSIONS

In this contribution, we described a method for time-wise retrieval of BR-DCBs employing code measurements simultaneously collected by two receivers forming one zero-baseline from GNSS constellations transmitting CDMA signals. These time-wise estimates of the BR-DCBs have therefore the same high temporal resolution as the collected GNSS measurements. We described two statistical hypothesis testing schemes with the goal of testing, respectively, the intra-day stability of time-wise estimates of the BR-DCBs and the consistency between the DWA estimates of the GEO/IGSO/MEO BR-DCBs.

We carried out a field campaign over an entire 1-year period (2013) at the main campus of Curtin University in Bentley (Perth), during which, dual-frequency GPS/BeiDou/Galileo measurements were collected by four receivers of three types connected to one common antenna, with a sampling rate of 30 seconds. We defined three independent receiver-pairs and for each of them we retrieved the time-wise estimates of GPS/GEO/IGSO/MEO/Galileo BR-DCBs. The main conclusions drawn from analyzing these BR-DCB estimates include:

- For each group of BR-DCB estimates, they are sufficiently stable over a 1-day period;
- For receiver-pairs of mixed type, possible inconsistency between GEO/IGSO/MEO BR-DCB estimates may occur, mainly due to the effect of BeiDou code ISTBs;
- The DWA estimates of BR-DCBs may exhibit an abrupt change induced by receiver firmware upgrades, whose size can range from 0.4 ns to 0.5 ns;
- The variability in the DWA estimates of the BR-DCBs over a 1-year period shows a high correlation with the daily maximum temperature variations at receiver sites.

ACKNOWLEDGMENTS

This work has been executed in the framework of the Positioning Program Project 1.01 ”New carrier phase processing strategies for achieving precise and reliable multi-satellite, multi-frequency GNSS/RNSS positioning in Australia” of the Cooperative Research Centre for Spatial Information (CRC-SI). This work was also partially funded by the CAS/KNAW joint research project ‘Compass, Galileo and GPS for improved ionosphere modeling’. The second author is the recipient of an Australian Research Council (ARC) Federation Fellowship (project number FF0883188). All this support is gratefully acknowledged.

REFERENCES

[1] Hernández-Pajares, M., et al., *The ionosphere: effects, GPS modeling and the benefits for space geodetic techniques.* Journal of Geodesy, 2011. **85**(12): p. 887-907.

[2] Jin, S. and A. Komjathy, *GNSS reflectometry and remote sensing: New objectives and results.* Advances in Space Research, 2010. **46**(2): p. 111-117.

[3] Jakowski, N., et al., *Ionospheric space weather effects monitored by simultaneous ground and space based GNSS signals.* Journal of atmospheric and solar-terrestrial physics, 2005. **67**(12): p. 1074-1084.

[4] Yiyan, Z., et al., *Ionospheric anomalies detected by ground-based GPS before the Mw7. 9 Wenchuan earthquake of May 12, 2008, China.* Journal of atmospheric and solar-terrestrial physics, 2009. **71**(8): p. 959-966.

[5] Zakharenkova, I., et al., *Anomalous modification of the ionospheric total electron content prior to the 26 September 2005 Peru earthquake.* Journal of atmospheric and solar-terrestrial physics, 2008. **70**(15): p. 1919-1928.

[6] Banville, S., et al., *Global and Regional Ionospheric Corrections for Faster PPP Convergence.* Navigation, 2014. **61**(2): p. 115-124.

[7] Montenbruck, O., P. Steigenberger, and A. Hauschild, *Broadcast versus precise ephemerides: a multi-GNSS perspective.* GPS Solutions, 2014. DOI: 10.1007/s10291-014-0390-8.

[8] Yang, Y., et al., *Preliminary assessment of the navigation and positioning performance of BeiDou regional navigation satellite system.* Science China Earth Sciences, 2014. **57**(1): p. 144-152.

[9] Bartolomé, J.P., et al., *Overview of Galileo System*, in *GALILEO Positioning Technology* 2015, Springer. p. 9-33.

[10] Spits, J. and R. Warnant, *Total electron content monitoring using triple frequency GNSS: Results with Giove-A/-B data.* Advances in Space Research, 2011. **47**(2): p. 296-303.

[11] Spits, J. and R. Warnant, *Total electron content monitoring using triple frequency GNSS data: A three-step approach.* Journal of Atmospheric and Solar-Terrestrial Physics, 2008. **70**(15): p. 1885-1893.

[12] Hernández-Pajares, M., et al., *The IGS VTEC maps: a reliable source of ionospheric information since 1998.* Journal of Geodesy, 2009. **83**(3-4): p. 263-275.

[13] Keshin, M., *A new algorithm for single receiver DCB estimation using IGS TEC maps.* GPS Solutions, 2012. **16**(3): p. 283-292.

[14] Sardón, E. and N. Zarraoa, *Estimation of total electron content using GPS data: How stable are the differential satellite and receiver instrumental biases?* Radio Science, 1997. **32**(5): p. 1899-1910.

[15] Coco, D.S., et al., *Variability of GPS satellite differential group delay biases.* Aerospace and Electronic Systems, IEEE Transactions on, 1991. **27**(6): p. 931-938.

[16] Li, Z., et al., *Two-step method for the determination of the differential code biases of COMPASS satellites.* Journal of Geodesy, 2012. **86**(11): p. 1059-1076.

[17] Zhang, B., et al., *Extraction of line-of-sight ionospheric observables from GPS data using precise point positioning.* Science China Earth Sciences, 2012. **55**(11): p. 1919-1928.

[18] Coster, A., et al., *Accuracy of GPS total electron content: GPS receiver bias temperature dependence.* Radio Science, 2013. **48**(2): p. 190-196.

[19] Bruyninx, C., P. Defraigne, and J.-M. Sleewaegen, *Time and frequency transfer using GPS codes and carrier phases: onsite experiments.* GPS Solutions, 1999. **3**(2): p. 1-10.

[20] Ciraolo, L., et al., *Calibration errors on experimental slant total electron content (TEC) determined with GPS.* Journal of Geodesy, 2007. **81**(2): p. 111-120.

[21] Brunini, C. and F.J. Azpilicueta, *Accuracy assessment of the GPS-based slant total electron content.* Journal of Geodesy, 2009. **83**(8): p. 773-785.
[22] Brunini, C. and F. Azpilicueta, *GPS slant total electron content accuracy using the single layer model under different geomagnetic regions and ionospheric conditions.* Journal of Geodesy, 2010. **84**(5): p. 293-304.
[23] Conte, J.F., F. Azpilicueta, and C. Brunini, *Accuracy assessment of the GPS-TEC calibration constants by means of a simulation technique.* Journal of Geodesy, 2011. **85**(10): p. 707-714.
[24] Zhang, D., et al., *The variation of the estimated GPS instrumental bias and its possible connection with ionospheric variability.* Science China Technological Sciences, 2014. **57**(1): p. 67-79.
[25] Zhang, D., et al., *Accuracy analysis of the GPS instrumental bias estimated from observations in middle and low latitudes.* Annales Geophysicae, 2010. **28**: p. 1571-1580.
[26] Kao, S., et al., *Factors affecting the estimation of GPS receiver instrumental biases.* Survey Review, 2013. **45**(328): p. 59-67.
[27] de Bakker, P.F., et al., *Short and zero baseline analysis of GPS L1 C/A, L5Q, GIOVE E1B, and E5aQ signals.* GPS solutions, 2012. **16**(1): p. 53-64.
[28] Nadarajah, N., P.J. Teunissen, and N. Raziq, *BeiDou inter-satellite-type bias evaluation and calibration for mixed receiver attitude determination.* Sensors, 2013. **13**(7): p. 9435-9463.
[29] Sleewaegen, J.-M., 2015, Private communication.
[30] Teunissen, P. and A. Khodabandeh. *Do GNSS parameters always benefit from integer ambiguity resolution? A PPP-RTK Network Scenario*. in *Proceedings of the 27th International Technical Meeting of The Satellite Division of the Institute of Navigation (ION GNSS+ 2014)*. Tampa, Florida, September 2014: p. 590-600.
[31] Odolinski, R., P.J. Teunissen, and D. Odijk, *Combined BDS, Galileo, QZSS and GPS single-frequency RTK.* GPS Solutions, 2015. **19**(1): p. 151-163.
[32] Teunissen, P., R. Odolinski, and D. Odijk, *Instantaneous BeiDou+ GPS RTK positioning with high cut-off elevation angles.* Journal of Geodesy, 2014. **88**(4): p. 335-350.
[33] Warnant, R., *Reliability of the TEC computed using GPS measurements—the problem of hardware biases.* Acta Geodaetica et Geophysica Hungarica, 1997. **32**(3-4): p. 451-459.
[34] Choi, B.-K., et al., *Comparison of GPS receiver DCB estimation methods using a GPS network.* Earth Planets Space, 2013. **65**(7): p. 707-711.
[35] Montenbruck, O., 2015, Private communication.